Journal of Molecular Science

Journal of Molecular Science
Volume 36 Issue 2, Year of Publication 2026, Page 521-528
DoI-10.004687/1000-9035.2026.062

Journal of Molecular Science
www.jmolecularsci.com ISSN:1000-9035

Quality-by-Design-Based Development and Physicochemical Characterization of Terbinafine Hydrochloride-Loaded Nanostructured Lipid Carriers Optimized Using Box–Behnken Design

Mahak Modi [1*], Phool Singh Yaduwanshi[2]
[1]*Research Scholar, Department of Pharmacy, IES University, Bhopal (M.P.) 462044, India.
[2] Professor, IITM, Department of Pharmacy, IES University, Bhopal (M.P.), 462044, India.

Article Information
Received: 21-05-2026
Revised: 04-06-2026
Accepted: 18-06-2026
Published: 08-07-2026

Keywords
terbinafine hydrochloride; nanostructured lipid carriers; Box–Behnken design; Quality by Design; onychomycosis; nanoparticle optimization.

ABSTRACT
Terbinafine hydrochloride, a first-line allylamine antifungal for onychomycosis, is limited clinically by poor aqueous solubility, high keratin-binding affinity, and negligible penetration through the dense keratinized nail plate. The present study aimed to develop and systematically optimize terbinafine-loaded nanostructured lipid carriers (NLCs) to overcome these biopharmaceutical limitations and provide a rational lipid-based platform for subsequent transungual delivery. Pre-formulation studies confirmed drug identity and purity by UV spectroscopy (λmax 222 nm), FTIR, and melting-point analysis (204–208 °C), while solubility and partition-coefficient studies established the drug's marked lipophilicity (log P ≈ 3.28–3.3) and preferential solubility in lipidic vehicles such as oleic acid and Capryol 90. Drug–excipient compatibility, verified by FTIR and differential scanning calorimetry (DSC), showed retention of all characteristic drug peaks without new peak formation, confirming the absence of chemical interaction with Compritol® 888 ATO, oleic acid, Poloxamer 188, soy lecithin, and chitosan. NLCs were fabricated by melt emulsification coupled with ultrasonication and high-pressure homogenization, and the formulation was optimized using a three-factor, three-level Box–Behnken design with Compritol® 888 ATO, oleic acid, and Poloxamer 188 concentrations as independent variables and particle size, polydispersity index (PDI), and entrapment efficiency as dependent responses. Quadratic models for all responses were statistically significant ($p < 0.001$, $R^2 > 0.95$). The desirability-optimized formulation (4.0% Compritol® 888 ATO, 1.7% oleic acid, 2.6% Poloxamer 188) yielded nanoparticles of 185.1 ± 2.4 nm with a PDI of 0.246 ± 0.02, zeta potential of −26.8 ± 1.1 mV, and entrapment efficiency of 87.2 ± 1.4%, in close agreement with model predictions (desirability = 0.982). Scanning and transmission electron microscopy revealed spherical, smooth-surfaced nanoparticles, while DSC and X-ray diffraction confirmed a reduction in drug crystallinity consistent with molecular dispersion within the imperfect lipid matrix characteristic of NLCs. These findings establish a reproducible, statistically validated, and stable terbinafine-NLC platform suitable for further performance evaluation as a topical antifungal delivery system.

1. INTRODUCTION:

Onychomycosis is a chronic fungal infection of the nail unit, accounting for up to half of all nail disorders worldwide, with markedly elevated prevalence in warm, humid regions such as India (Lipner & Scher, 2023; Veeranna & Shashikumar, 2021). Beyond its physical manifestations, the condition imposes a substantial psychosocial and economic burden, is prone to relapse, and remains difficult to eradicate because the causative dermatophytes—chiefly Trichophyton rubrum and

Journal of Molecular Science
Volume 36 Issue 2, Year of Publication 2026, Page 521-528
DoI-10.004687/1000-9035.2026.062

T. mentagrophytes—establish themselves within an avascular, densely keratinized nail plate that is intrinsically resistant to drug penetration (Elkeeb, Hui, & Maibach, 2010; Sigurgeirsson & Baran, 2014).

Terbinafine hydrochloride, an allylamine that fungicidally inhibits squalene epoxidase, is widely regarded as the drug of choice for dermatophyte onychomycosis owing to its potent, rapidly cidal activity and favourable safety profile relative to azoles (Ryder, 1992; Gupta & Simpson, 2018). However, its clinical utility is constrained by unfavourable biopharmaceutical properties: practical insolubility in water, high lipophilicity (log P ≈ 3.3–5.5), strong keratin-binding affinity that sequesters the drug superficially, and consequent poor transungual flux from conventional topical vehicles, which achieve complete cure rates below 15–20% (Elewski et al., 2013; Monti, Sacchetti, & Mailland, 2012). Oral therapy circumvents nail-plate impermeability but introduces systemic exposure, hepatotoxicity risk, and drug–drug interaction liability that limit its use in vulnerable populations (Piraccini & Sisti, 2015).

Nanostructured lipid carriers (NLCs) represent a second-generation lipid nanocarrier platform in which a blend of solid and liquid lipids forms a structurally imperfect matrix, in contrast to the ordered crystalline lattice of first-generation solid lipid nanoparticles (SLNs). This imperfection creates additional space for drug accommodation, increases entrapment efficiency, minimizes drug expulsion on storage, and improves adhesion to keratinized tissue through sebum-mimetic liquid-lipid components (Müller, Radtke, & Wissing, 2002; Pardeike, Hommoss, & Müller, 2009; Das & Chaudhury, 2019). Given terbinafine's high lipophilicity and strong compatibility with lipidic environments, NLCs are a rational, biocompatible vehicle for enhancing its solubilization, stability, and nail-directed delivery (Gupta, Vyas, & Vyas, 2020; Lasoń, Sikora, & Miastkowska, 2021).

Empirical, trial-and-error formulation of lipid nanocarriers frequently yields inconsistent particle size, entrapment efficiency, and stability, and the literature reflects limited use of systematic Design-of-Experiments (DoE) approaches for terbinafine-loaded NLCs specifically (Patel, Patel, & Patel, 2021; Saini, Kumar, & Sharma, 2023). A Quality-by-Design (QbD) framework, in which critical formulation variables are varied systematically and their effects on critical quality attributes are modelled statistically, offers a more rigorous and reproducible path to an optimized nanoparticle system than single-variable optimization.

The present study therefore aimed to develop terbinafine hydrochloride-loaded NLCs using a rationally selected lipid–surfactant combination, to optimize the formulation using a three-factor, three-level Box–Behnken design (BBD) with particle size, polydispersity index, and entrapment efficiency as critical quality attributes, and to comprehensively characterize the resulting optimized nanoparticles with respect to their physicochemical, morphological, thermal, and crystalline properties. This paper reports the formulation-development and optimization component of a broader investigation; the ex vivo permeation, antifungal, and stability performance of the optimized NLC system are addressed separately.

2. MATERIALS AND METHODS:

2.1. Materials:

Terbinafine hydrochloride was procured from Sigma-Aldrich and used as received. Compritol® 888 ATO, stearic acid, glyceryl monostearate, and Precirol® ATO 5 were evaluated as candidate solid lipids (Gattefossé). Oleic acid, Capryol® 90, and isopropyl myristate served as candidate liquid lipids. Poloxamer 188, Tween 80, Span 60, and soy lecithin were used as surfactants/co-surfactants, and chitosan (low molecular weight) was employed as a mucoadhesive polymeric coating. Analytical-grade methanol, ethanol, and acetonitrile, and standard phosphate buffer salts, were used for analytical work. Trichophyton rubrum and Trichophyton mentagrophytes (MTCC) were reserved for the antifungal-evaluation phase of the broader study and are not reported here.

2.2. Drug Identification and Preformulation Analysis:

The identity and purity of terbinafine hydrochloride were confirmed by UV spectrophotometric scanning (200–400 nm) of a 10 µg/mL methanolic solution to determine λmax, followed by construction of a calibration curve (2–10 µg/mL) at the determined λmax. FTIR spectra were acquired by the KBr pellet method (4000–400 cm^{-1}) to confirm characteristic functional-group absorptions. Melting point was determined in triplicate by the capillary method using a digital melting-point apparatus.

Equilibrium solubility of terbinafine hydrochloride in water, methanol, ethanol, phosphate buffer (pH 6.8), oleic acid, and Capryol® 90 was determined by the shake-flask method (24 h, room temperature, orbital shaking), followed by centrifugation, filtration, and spectrophotometric assay at λmax. The n-octanol–water partition coefficient (log P) was determined using mutually pre-saturated phases shaken for 24 h at room temperature, with drug concentration in the aqueous phase quantified spectrophotometrically and the octanol-phase

Journal of Molecular Science
Volume 36 Issue 2, Year of Publication 2026, Page 521-528
DoI-10.004687/1000-9035.2026.062

concentration obtained by mass balance.

2.3. Drug–Excipient Compatibility Studies:
Physical mixtures of terbinafine hydrochloride with each selected excipient (Compritol® 888 ATO, oleic acid, Poloxamer 188, soy lecithin, and chitosan) were prepared in the ratios intended for the final formulation. FTIR spectra of the pure drug, individual excipients, and physical mixtures were compared for peak retention, shift, or disappearance. DSC thermograms were recorded from 30 °C to 300 °C at a heating rate of 10 °C/min under a nitrogen atmosphere (Mettler Toledo DSC) for the same set of samples to assess thermal compatibility.

2.4. Experimental Design for Formulation Optimization:
A three-factor, three-level Box–Behnken design (Design-Expert® software) was employed to optimize the NLC formulation with a reduced number of experimental runs relative to a full factorial design while still enabling estimation of quadratic and interaction effects. The independent variables were solid lipid concentration (Compritol® 888 ATO, A: 3–5% w/w), liquid lipid concentration (oleic acid, B: 1–2% w/w), and surfactant concentration (Poloxamer 188, C: 1–3% w/w); terbinafine HCl (1.0%), soy lecithin (1.0%), and chitosan (0.5%) were held constant across all runs. Particle size (Y1), polydispersity index (Y2), zeta potential, entrapment efficiency (Y3), and drug release at 12 h (Y4) were recorded as dependent responses. Fifteen experimental runs, including three centre-point replicates, were generated and executed in randomized order (Table 1). Second-order polynomial models were fitted to each response, and model adequacy was assessed by analysis of variance (ANOVA), coefficient of determination (R^2 and adjusted R^2), and lack-of-fit testing. Numerical optimization was performed using the desirability function, with constraints set to minimize particle size and PDI and maximize entrapment efficiency and drug release.

2.5. Preparation of Terbinafine-Loaded NLCs:
NLCs were prepared by melt emulsification combined with probe ultrasonication and high-pressure homogenization. Briefly, Compritol® 888 ATO and oleic acid were melted together at 75 ± 2 °C, and terbinafine hydrochloride was dissolved in the molten lipid phase under continuous stirring; soy lecithin was incorporated to aid emulsification. An aqueous phase containing Poloxamer 188 was heated to the same temperature and added slowly to the lipid phase under high-speed stirring (10,000–15,000 rpm, 15 min) to form a coarse oil-in-water emulsion. The coarse emulsion was subjected to probe ultrasonication (60% amplitude, 30 s on/10 s off pulse cycle, 8 min, maintained below 30 °C) and then to high-pressure homogenization (1000 bar, 4 cycles, 70 °C). The resulting hot nanoemulsion was cooled to room temperature under continuous stirring to allow lipid recrystallization and NLC formation, after which a chitosan solution (prepared in 1% v/v acetic acid) was added slowly under gentle stirring to coat the nanoparticles.

2.6. Characterization of Optimized NLCs:
Mean particle size, PDI, and zeta potential were measured by dynamic light scattering (Malvern Zetasizer) at 25 °C following appropriate dilution with distilled water. Entrapment efficiency and drug loading were determined by centrifugation (15,000 rpm, 30 min) to separate unentrapped drug, with the free drug in the supernatant quantified by UV spectrophotometry at 222 nm; entrapment efficiency and drug loading were calculated from the difference between total and free drug relative to the lipid mass. Particle morphology was examined by scanning electron microscopy (SEM) and transmission electron microscopy (TEM). Thermal behaviour and crystallinity of the optimized formulation, in comparison with the pure drug, were assessed by DSC (30–300 °C, 10 °C/min, nitrogen atmosphere).

2.7. Statistical Analysis:
All experimental data are expressed as mean ± standard deviation (SD) of at least triplicate determinations unless otherwise stated. Response-surface regression, ANOVA, and desirability-based numerical optimization were performed using Design-Expert® software; a model was considered statistically significant at $p < 0.05$.

3. RESULTS AND DISCUSSION:

3.1. Drug Identification and Preformulation Characteristics:
The UV absorption spectrum of terbinafine hydrochloride in methanol showed a sharp, well-defined λmax at 222 nm, consistent with literature values and attributable to the π→π* transition of the drug's conjugated naphthalene system. The calibration curve constructed at this wavelength (2–10 µg/mL) was linear, with a regression equation of $y = 0.075x + 0.002$ and $R^2 = 0.9994$, confirming adherence to the Beer–Lambert law and validating the method for subsequent quantitative work (Table 1).

Table 1. Calibration Data of Terbinafine HCl in Methanol (λmax = 222 nm)

Concentration (µg/mL)	Absorbance (AU)
2	0.152
4	0.301
6	0.452
8	0.598
10	0.751

Journal of Molecular Science
Volume 36 Issue 2, Year of Publication 2026, Page 521-528
DoI-10.004687/1000-9035.2026.062

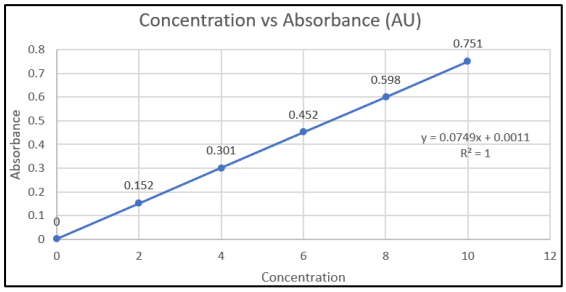

Fig 1

FTIR analysis of the pure drug showed all expected characteristic absorptions, including aromatic C–H stretching (~3050 cm^{-1}), aliphatic C–H stretching (~2920 cm^{-1}), a diagnostic C≡C alkyne stretch (~2200 cm^{-1}) unique to terbinafine's structure, aromatic C=C stretching (~1600 cm^{-1}), and C–N stretching of the amine group (~1100 cm^{-1}), with no extraneous peaks indicative of impurities. The melting point, determined by the capillary method, fell within a narrow range of 204–208 °C, consistent with reported values and indicative of high drug purity. Together, these results confirmed the identity, purity, and suitability of the procured terbinafine hydrochloride for formulation development.

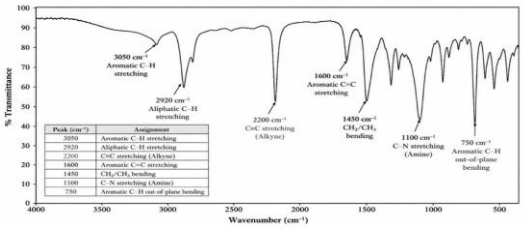

FTIR of Terbinafine Hydrochloride sampled drug

Fig 2

3.2. Solubility and Partition Coefficient:

Terbinafine hydrochloride displayed extremely poor aqueous solubility (0.002 mg/mL in water; 0.015 mg/mL in phosphate buffer pH 6.8), consistent with its BCS Class II classification, while showing markedly higher solubility in organic solvents and, notably, in lipid vehicles—30.2 mg/mL in Capryol® 90 and 25.4 mg/mL in oleic acid (Table 2). This pronounced preference for lipidic media provided direct experimental justification for selecting a lipid-based nanocarrier system rather than an aqueous or polymeric vehicle.

The n-octanol–water partition coefficient was calculated as log P ≈ 3.28, in agreement with literature values of 3.3–3.5 for terbinafine hydrochloride, confirming its high lipophilicity. This log P value indicates strong thermodynamic compatibility with lipid matrices and supports the expectation of high entrapment efficiency within a solid–liquid lipid blend, since lipophilic drugs of this magnitude typically partition preferentially into the oily domains created by the liquid-lipid component of an NLC rather than remaining at the aqueous interface (Gupta, Vyas, & Vyas, 2020).

Table 2. Solubility Profile of Terbinafine Hydrochloride in Various Solvents and Lipid Vehicles

Solvent / Vehicle	Solubility (mg/mL)	Classification
Water	0.002	Practically insoluble
Phosphate buffer (pH 6.8)	0.015	Slightly soluble
Ethanol	8.2	Soluble
Methanol	12.5	Freely soluble
Oleic acid	25.4	Very freely soluble
Capryol® 90	30.2	Very freely soluble

3.3. Drug–Excipient Compatibility (FTIR and DSC):

FTIR spectra of the physical mixture of terbinafine hydrochloride with Compritol® 888 ATO, oleic acid, Poloxamer 188, soy lecithin, and chitosan retained all characteristic drug peaks, including the diagnostic alkyne C≡C stretch at ~2200 cm^{-1}, without shift or disappearance; only minor peak broadening attributable to spectral overlap of excipient bands was observed. This pattern is consistent with a purely physical admixture and indicates the absence of chemical interaction between the drug and the selected excipients.

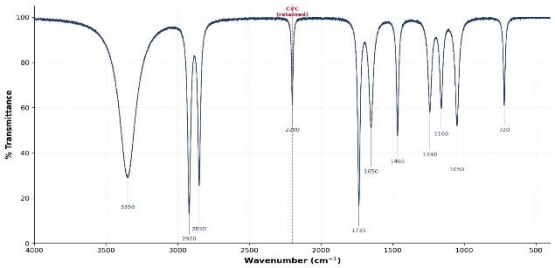

Fig 3

DSC thermograms corroborated this conclusion. Pure terbinafine hydrochloride exhibited a sharp endothermic melting peak at 204–208 °C, while Compritol® 888 ATO, oleic acid, Poloxamer 188, soy lecithin, and chitosan showed their own characteristic thermal transitions at 70–75 °C, ~55–60 °C, 50–60 °C, ~100–120 °C, and 80–150 °C, respectively (Table 3). In the physical mixture, the drug's melting endotherm was retained at a comparable temperature but with reduced intensity and slight broadening—changes attributable to partial dispersion of the drug within the lipid phase rather than chemical incompatibility, since no new thermal events or peak disappearances were observed. These findings collectively validated the compatibility of all selected components and provided the basis for proceeding to nanoparticle fabrication.

Journal of Molecular Science
Volume 36 Issue 2, Year of Publication 2026, Page 521-528
DoI-10.004687/1000-9035.2026.062

Table 3. DSC Thermal Events of Pure Drug, Excipients, and Physical Mixture

Component	Thermal Transition (°C)	Interpretation
Terbinafine HCl	204–208	Sharp melting endotherm; crystalline
Compritol® 888 ATO	70–75	Lipid melting peak
Oleic acid	~55–60	Melting transition
Poloxamer 188	50–60	Gel–liquid transition
Soy lecithin	~100–120	Phospholipid phase behaviour
Chitosan	80–150	Moisture loss / polymer relaxation
Physical mixture	204–208 (reduced intensity)	Drug peak retained; no new peaks

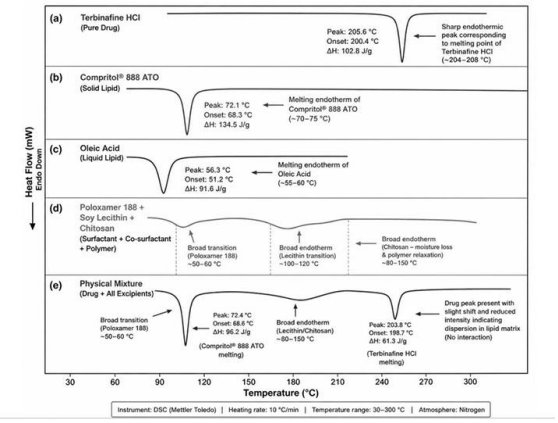

Fig 4

3.4. Box–Behnken Design: Composition and Rationale of Selected Components:

Compritol® 888 ATO (glyceryl behenate) was selected as the solid lipid for its high melting point, biocompatibility, and capacity to form an imperfect crystalline matrix favourable for drug accommodation. Oleic acid was selected as the liquid lipid for its high solubilizing capacity for terbinafine and its established role as a nail- and skin-penetration enhancer, and for its ability to disrupt lipid crystallinity when blended with the solid lipid. Poloxamer 188 was chosen as the primary surfactant for its low toxicity and efficient steric stabilization of the nanoparticle surface, with soy lecithin included as a co-surfactant to improve interfacial film formation, and chitosan incorporated as a bioadhesive coating to promote interaction with the negatively charged nail keratin. This rationally selected five-component system (drug, solid lipid, liquid lipid, surfactant, co-surfactant/coating) was then carried into the Box–Behnken optimization.

3.5. Effect of Formulation Variables on Particle Size and Entrapment Efficiency:

Across the fifteen Box–Behnken runs, particle size ranged from 176.8 nm (F7) to 289.5 nm (F6), and entrapment efficiency ranged from 71.2% (F1) to 91.5% (F8) (Table 4). The fitted second-order polynomial for particle size (Y1) was:

$$Y1 = 185.63 + 31.42A - 18.37B - 24.51C + 6.28AB + 4.17AC - 2.84BC$$

Increasing Compritol® 888 ATO concentration (A) significantly increased particle size, consistent with the higher viscosity and greater bulk of a denser solid-lipid phase resisting size reduction during homogenization. In contrast, increasing Poloxamer 188 concentration (C) reduced particle size by lowering interfacial tension and providing more effective steric stabilization, while oleic acid (B) reduced particle size by introducing fluidity and lattice imperfections that facilitated more efficient emulsification.

The fitted model for entrapment efficiency (Y2) was:

$$Y2 = 87.00 + 5.84A + 3.16B + 4.48C - 1.24AB + 0.76AC + 0.58BC$$

All three variables positively influenced entrapment efficiency. Higher solid-lipid content provided a more extensive matrix capable of accommodating a greater drug payload; oleic acid introduced structural imperfections in the crystalline lattice that created additional cavities for drug incorporation—the defining structural advantage of NLCs over conventional SLNs; and Poloxamer 188 contributed by forming a stabilizing shell that reduced drug expulsion during lipid recrystallization. These opposing trends—particle-size reduction with Poloxamer 188 versus entrapment gains with Compritol® 888 ATO—illustrate the classical trade-off in lipid nanoparticle optimization and underscore the necessity of a multi-response DoE approach rather than single-factor optimization.

Table 4. Box–Behnken Design Matrix and Observed Responses

Run	A: Compritol® (%)	B: Oleic acid (%)	C: Poloxamer 188 (%)	Particle size (nm)	PDI	Zeta potential (mV)	EE (%)
F1	3	1	2	221.4	0.362	-18.6	71.2
F2	5	1	2	276.3	0.401	-21.5	86.5
F3	3	2	2	194.2	0.298	-24.3	79.8
F4	5	2	2	251.8	0.336	-25.7	89.1
F5	3	1.5	1	232.7	0.418	-19.8	74.6
F6	5	1.5	1	289.5	0.447	-22.1	84.2
F7	3	1.5	3	176.8	0.241	-27.6	81.3
F8	5	1.5	3	218.6	0.284	-29.2	91.5
F9	4	1	1	248.1	0.392	-20.6	76.8

Journal of Molecular Science
Volume 36 Issue 2, Year of Publication 2026, Page 521-528
DoI-10.004687/1000-9035.2026.062

F10	4	2	1	214.9	0.341	-23.4	82.5
F11	4	1	3	189.7	0.256	-28.3	84.1
F12	4	2	3	198.5	0.262	-30.5	90.2
F13	4	1.5	2	186.4	0.248	-26.4	86.8
F14	4	1.5	2	184.9	0.244	-26.7	87.2
F15	4	1.5	2	185.6	0.246	-26.5	87.0

3.6. Statistical Validation of the Optimization Models (ANOVA):

ANOVA confirmed that the quadratic model was highly significant for all four responses ($p < 0.001$ for three of four responses; $p = 0.0002$ for PDI), with R^2 values exceeding 0.95 and adjusted R^2 values exceeding 0.93 in every case (Table 5), indicating excellent goodness-of-fit and negligible unexplained variance. The close agreement between R^2 and adjusted R^2 for each response further indicated that the models were not over-fitted, supporting their use for reliable prediction and numerical optimization of the formulation.

Table 5. ANOVA Summary for Box–Behnken Design Responses

Response	Model F-value	p-value	R^2	Adjusted R^2
Particle size (Y1)	42.18	<0.0001	0.978	0.961
PDI (Y2)	31.44	0.0002	0.956	0.934
Entrapment efficiency (Y3)	38.26	<0.0001	0.971	0.952
Drug release at 12 h (Y4)	36.15	<0.0001	0.968	0.947

3.7. Numerical Optimization and Validation of the Optimized Formulation:

Numerical optimization using the desirability function, constrained to minimize particle size and PDI while maximizing entrapment efficiency and drug release, identified an optimal composition of 4.0% Compritol® 888 ATO, 1.7% oleic acid, and 2.6% Poloxamer 188 (with fixed 1.0% terbinafine HCl, 1.0% soy lecithin, and 0.5% chitosan; Table 6), yielding an overall desirability score of 0.982.

Experimental preparation and evaluation of this optimized composition showed excellent agreement with model predictions across all responses, with percentage deviations below 2% in every case (Table 7). This close concordance between predicted and observed values validates the predictive accuracy of the Box–Behnken models and confirms the robustness of the design-of-experiments approach for this formulation system.

Table 6. Optimized NLC Formulation Composition (Desirability = 0.982)

Component	Optimized Quantity (% w/w)
Terbinafine HCl	1.0
Compritol® 888 ATO	4.0
Oleic acid	1.7
Poloxamer 188	2.6
Soy lecithin	1.0
Chitosan	0.5
Distilled water	q.s. to 100 mL

Table 7. Validation of the Optimized Formulation: Predicted vs. Experimental Values

Parameter	Predicted value	Experimental value
Particle size (nm)	183.5	185.1 ± 2.4
PDI	0.241	0.246 ± 0.02
Zeta potential (mV)	−27.1	−26.8 ± 1.1
Entrapment efficiency (%)	87.6	87.2 ± 1.4
Drug release at 12 h (%)	88.7	88.1 ± 1.8

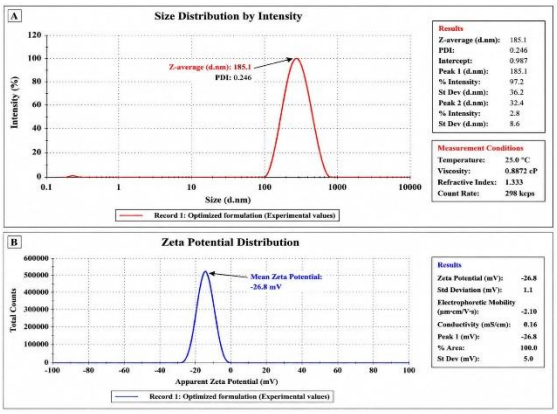

Fig 5

3.8. Particle Size, Polydispersity Index, and Zeta Potential of the Optimized NLCs:

Dynamic light scattering analysis of the optimized formulation confirmed a mean particle size of 185.1 ± 2.4 nm, within the nanoscale range generally considered favourable for engagement with the fine keratin channels and microfractures of the nail plate. The PDI of 0.246 ± 0.02 indicated a narrow, homogeneous size distribution—well within the threshold (<0.3) conventionally regarded as acceptable for pharmaceutical nanoparticulate systems—reflecting the efficiency of the combined ultrasonication and high-pressure homogenization process and the stabilizing action of Poloxamer 188 and soy lecithin at the particle surface.

The zeta potential of −26.8 ± 1.1 mV indicated adequate electrostatic repulsion between particles, consistent with a colloidally stable dispersion resistant to aggregation. The negative surface charge is attributable principally to the anionic carboxylate groups of oleic acid at the particle surface; the inclusion of chitosan, a cationic polymer, was deliberately balanced in the formulation to provide bioadhesive benefit without inducing excessive charge neutralization or reversal.

Journal of Molecular Science
Journal of Molecular Science
Volume 36 Issue 2, Year of Publication 2026, Page 521-528
DoI-10.004687/1000-9035.2026.062

3.9. Entrapment Efficiency and Drug Loading:

The optimized NLC formulation exhibited a high entrapment efficiency of 87.2 ± 1.4% and a drug loading of 14.8 ± 0.9%. This high entrapment is consistent with the marked lipophilicity of terbinafine (log P ≈ 3.28) established in the preformulation studies and its correspondingly high solubility in both the solid (Compritol® 888 ATO) and liquid (oleic acid) lipid components. The structural imperfections introduced into the crystalline lattice by the solid–liquid lipid blend provide additional molecular-scale vacancies for drug accommodation, a mechanistic advantage of NLCs over first-generation SLNs, whose more ordered lattice inherently constrains drug loading capacity (Müller, Radtke, & Wissing, 2002; Pardeike, Hommoss, & Müller, 2009).

3.10. Morphological Characterization (SEM and TEM):

SEM micrographs of the optimized NLCs revealed discrete, spherical particles with smooth surfaces and minimal inter-particle aggregation, consistent with the narrow PDI obtained by dynamic light scattering; this uniform surface morphology is attributable to a continuous Poloxamer 188 stabilizer layer enveloping the particles. TEM imaging confirmed the nanosized dimensions and revealed a core–shell-type internal architecture typical of NLCs, comprising a solid–liquid lipid core surrounded by a thin surfactant/lecithin interfacial layer. Particle sizes estimated from TEM images were in close agreement (within ±10%) with DLS measurements, and the absence of needle-like crystalline structures in the micrographs was consistent with amorphous or partially amorphous dispersion of the drug within the lipid matrix.

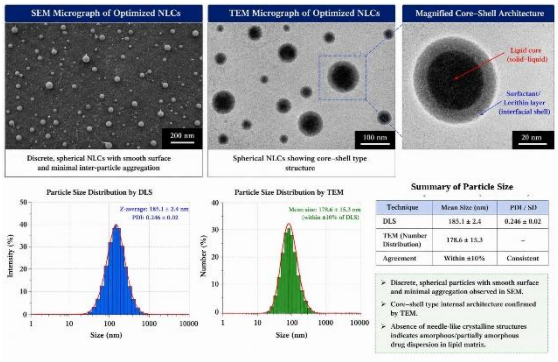

Fig 6

3.11. Thermal Behaviour and Crystallinity of the Optimized Formulation (DSC and XRD):

The DSC thermogram of pure terbinafine hydrochloride displayed a sharp endothermic peak at 204–208 °C, characteristic of its crystalline state. The corresponding peak in the optimized NLC formulation was markedly reduced in intensity and broadened, indicating a substantial reduction in drug crystallinity and successful molecular- or nanocrystalline-level dispersion of terbinafine within the lipid matrix. The Compritol® 888 ATO melting peak was also shifted slightly downward relative to the pure lipid, consistent with lattice disruption by the incorporated oleic acid—a signature thermal feature of the NLC's imperfect-matrix structure. No new endothermic or exothermic events were observed in the formulation thermogram, reaffirming the absence of drug–excipient chemical interaction under thermal stress.

Powder XRD corroborated these findings: pure terbinafine hydrochloride exhibited sharp, high-intensity diffraction peaks characteristic of a well-ordered crystal lattice, whereas the optimized NLC formulation showed markedly reduced peak intensity and a partial diffuse halo pattern, consistent with a loss of long-range crystalline order. This amorphous or nanocrystalline drug state within the lipid matrix is expected to favour more rapid and complete dissolution relative to the fully crystalline drug, since the energetic barrier associated with breaking a crystal lattice is substantially diminished when the drug is dispersed within an imperfect, semi-ordered lipid environment.

4. CONCLUSION:

A terbinafine hydrochloride-loaded nanostructured lipid carrier system was successfully developed and optimized using a Quality-by-Design approach. Preformulation studies confirmed the drug's identity, purity, marked lipophilicity, and compatibility with the selected lipid, surfactant, and polymeric excipients. A three-factor Box–Behnken design enabled systematic, statistically validated optimization of particle size and entrapment efficiency, yielding a formulation (4.0% Compritol® 888 ATO, 1.7% oleic acid, 2.6% Poloxamer 188) with a particle size of 185.1 ± 2.4 nm, PDI of 0.246 ± 0.02, zeta potential of −26.8 ± 1.1 mV, and entrapment efficiency of 87.2 ± 1.4%, all in close agreement with model predictions. Morphological and thermal analyses confirmed spherical nanoparticle architecture and a reduction in drug crystallinity consistent with successful dispersion within the imperfect lipid matrix. Collectively, these results establish a reproducible, well-characterized, and mechanistically rational terbinafine-NLC platform. The transungual permeation, antifungal, and stability performance of this optimized formulation are reported separately.

ACKNOWLEDGEMENTS

The authors acknowledge the Department of Pharmaceutics, Shri Ram Institute of Technology – Pharmacy, Jabalpur, for providing the facilities used in this study.

Journal of Molecular Science
Volume 36 Issue 2, Year of Publication 2026, Page 521-528
DoI-10.004687/1000-9035.2026.062

https://doi.org/10.18203/2320-6012.ijrms20210471

CONFLICT OF INTEREST:

The authors declare no conflict of interest.

REFERENCES:

1. Das, S., & Chaudhury, A. (2019). Recent advances in lipid nanoparticle formulations with solid matrix for combination drug therapy. European Journal of Pharmaceutics and Biopharmaceutics, 132, 78–89. https://doi.org/10.1016/j.ejpb.2018.09.016
2. Elewski, B. E., Leyden, J., Rinaldi, M. G., & Zasada, G. (2013). Onychomycosis: Current trends in diagnosis and treatment. Cutis, 91(6), 297–304.
3. Elkeeb, L., Hui, X., & Maibach, H. I. (2010). The nail plate: A potential target for drug delivery. Journal of Dermatological Science, 59(2), 65–71. https://doi.org/10.1016/j.jdermsci.2010.05.008
4. Gupta, A. K., & Simpson, F. C. (2018). New therapeutic options for onychomycosis. Expert Opinion on Pharmacotherapy, 19(7), 1–12. https://doi.org/10.1080/14656566.2018.1453746
5. Gupta, M., Vyas, S. P., & Vyas, A. (2020). Prospective nanotechnology-based strategies for the management of cutaneous fungal infections. Skin Pharmacology and Physiology, 33(5), 261–277. https://doi.org/10.1159/000509199
6. Lasoń, E., Sikora, E., & Miastkowska, M. (2021). Lipid nanocarriers for topical application: From production to clinical application. Pharmaceutics, 13(11), 1888. https://doi.org/10.3390/pharmaceutics13111888
7. Lipner, S. R., & Scher, R. K. (2023). Onychomycosis: Old and new. Journal of Fungi, 9(5), 559. https://doi.org/10.3390/jof9050559
8. Monti, D., Sacchetti, F., & Mailland, F. (2012). In vitro transungual permeation of terbinafine and ciclopirox from nail lacquers. Pharmaceutical Development and Technology, 17(7), 836–841. https://doi.org/10.3109/10837450.2011.590633
9. Müller, R. H., Radtke, M., & Wissing, S. A. (2002). Nanostructured lipid matrices for improved microencapsulation of drugs. International Journal of Pharmaceutics, 242(1–2), 121–128. https://doi.org/10.1016/S0378-5173(02)00180-1
10. Pardeike, J., Hommoss, A., & Müller, R. H. (2009). Lipid nanoparticles (SLN, NLC) in cosmetic and pharmaceutical dermal products. International Journal of Pharmaceutics, 366(1–2), 170–184. https://doi.org/10.1016/j.ijpharm.2008.07.003
11. Patel, R., Patel, P., & Patel, N. (2021). Current insights on antifungal therapy: Novel nanotechnology approaches for drug delivery systems and new drugs from natural sources. Pharmaceuticals, 13(9), 248. https://doi.org/10.3390/ph13090248
12. Piraccini, B. M., & Sisti, A. (2015). Drug-related adverse reactions of oral antifungals in onychomycosis. Expert Opinion on Drug Safety, 14(7), 1047–1055. https://doi.org/10.1517/14740338.2015.1049676
13. Ryder, N. S. (1992). Terbinafine: Mode of action and properties of squalene epoxidase inhibition. British Journal of Dermatology, 126(Suppl 39), 2–7.
14. Saini, P., Kumar, R., & Sharma, A. (2023). Contemporary techniques and potential transungual drug delivery approaches for the management of onychomycosis. AAPS PharmSciTech, 24(6), 142. https://doi.org/10.1208/s12249-023-02603-x
15. Sigurgeirsson, B., & Baran, R. (2014). The prevalence of onychomycosis in the global population—A systematic literature review. Journal of the European Academy of Dermatology and Venereology, 28(11), 1480–1491. https://doi.org/10.1111/jdv.12323
16. Veeranna, S. A., & Shashikumar, B. M. (2021). A study of etiology and epidemiology of onychomycosis from a tertiary care hospital in South India. International Journal of Research in Medical Sciences, 9(3), 918–924.